ARTICLES

Journal of Semiconductors
(2024) 45, 012101
doi: 10.1088/1674-4926/45/1/012101

Enhanced magnetic anisotropy and high hole mobility in magnetic semiconductor $Ga_{1-x-y}Fe_xNi_ySb$

Zhi Deng[1, 2], Hailong Wang[1, 2, †], Qiqi Wei[1, 2], Lei Liu[1, 2], Hongli Sun[1, 2], Dong Pan[1, 2], Dahai Wei[1, 2], and Jianhua Zhao[1, 2]

[1]State Key Laboratory of Superlattices and Microstructures, Institute of Semiconductors, Chinese Academy of Sciences, Beijing 100083, China
[2]Center of Materials Science and Optoelectronics Engineering, University of Chinese Academy of Sciences, Beijing 100190, China

Abstract: (Ga,Fe)Sb is a promising magnetic semiconductor (MS) for spintronic applications because its Curie temperature (T_C) is above 300 K when the Fe concentration is higher than 20%. However, the anisotropy constant K_u of (Ga,Fe)Sb is below 7.6×10^3 erg/cm^3 when Fe concentration is lower than 30%, which is one order of magnitude lower than that of (Ga,Mn)As. To address this issue, we grew $Ga_{1-x-y}Fe_xNi_ySb$ films with almost the same x (≈24%) and different y to characterize their magnetic and electrical transport properties. We found that the magnetic anisotropy of $Ga_{0.76-y}Fe_{0.24}Ni_ySb$ can be enhanced by increasing y, in which K_u is negligible at y = 1.7% but increases to 3.8×10^5 erg/cm^3 at y = 6.1% (T_C = 354 K). In addition, the hole mobility (μ) of $Ga_{1-x-y}Fe_xNi_ySb$ reaches 31.3 cm^2/(V·s) at x = 23.7%, y = 1.7% (T_C = 319 K), which is much higher than the mobility of $Ga_{1-x}Fe_xSb$ at x = 25.2% (μ = 6.2 cm^2/(V·s)). Our results provide useful information for enhancing the magnetic anisotropy and hole mobility of (Ga,Fe)Sb by using Ni co-doping.

Key words: magnetic semiconductor; molecular beam epitaxy; Fe-Ni co-doping; magnetic anisotropy; hole mobility

Citation: Z Deng, H L Wang, Q Q Wei, L Liu, H L Sun, D Pan, D H Wei, and J H Zhao, Enhanced magnetic anisotropy and high hole mobility in magnetic semiconductor $Ga_{1-x-y}Fe_xNi_ySb$[J]. *J. Semicond.*, 2024, 45(1), 012101. https://doi.org/10.1088/1674-4926/45/1/012101

1. Introduction

Magnetic semiconductors (MSs) are promising materials for spintronic applications, which would be useful for non-volatile and low-power-consumption electronic devices[1–5]. The ideal MSs are expected to at least satisfy the following requirements: first, their Curie temperature should be higher than room temperature (300 K); and second, both p-type and n-type MSs could be realized. Mn-based Ⅲ−Ⅴ MSs have been intensively investigated, such as p-type (In,Mn)As[6–10] and (Ga,Mn)As[11–15], while the maximum T_C are still much lower than room temperature (90 K in (In,Mn)As[10], 200 K in (Ga,Mn)As[13]). However, the effort made by previous research could not realize a MS satisfying these two requirements, until new results were found in Fe-doped Ⅲ−Ⅴ MSs. Both n- and p-type MSs could be achieved by doping Fe into Ⅲ−Ⅴ host semiconductors, such as p-type (Ga,Fe)Sb (with maximum T_C = 400 K)[16–20] and n-type (In,Fe)Sb (with maximum T_C = 385 K)[21–23]. Moreover, plenty of recent research has focused on the microscopic origin of the ferromagnetism of (Ga,Fe)Sb, revealing the intrinsic ferromagnetism of (Ga,Fe)Sb films[19, 20, 24–26].

The magnetic anisotropy of (Ga,Fe)Sb (7.6×10^3 erg/cm^3 at x_{Fe} = 29.8%) is much smaller than the typical value of (Ga,Mn)As (3.6×10^4 erg/cm^3)[27], which makes it difficult to be utilized for practical applications. In this work, we co-doped Ni with Fe into GaSb host semiconductor and achieved enhanced magnetic anisotropy of $Ga_{1-x-y}Fe_xNi_ySb$ films than that of (Ga,Fe)Sb. As a result, the K_u of $Ga_{1-x-y}Fe_xNi_ySb$ is negligible at y = 1.7% but increases to 3.8×10^5 erg/cm^3 at y = 6.1%, while the Curie temperature of samples was maintained above 300 K. Additionally, the hole mobility of $Ga_{1-x-y}Fe_xNi_ySb$ films reaches at 31.3 cm^2/(V·s) at x = 23.7%, y = 1.7%, which is much higher than the mobility of $Ga_{1-x}Fe_xSb$ at x = 25.2% (μ = 6.2 cm^2/(V·s)).

2. Experiments

The $Ga_{1-x-y}Fe_xNi_ySb$ films were grown on semi-insulating GaAs(001) substrates by low temperature molecular beam epitaxy (LT-MBE), a schematic sample structure is shown in Fig. 1(a). At first, we grew a 150-nm-thick GaAs buffer layer to obtain a smooth GaAs surface at 550 °C. Then, a 5-nm-thick AlSb was deposited at 470 °C as a seed layer, following with a 100-nm-thick $Al_{0.9}Ga_{0.1}Sb$ buffer layer grown at 470 °C to relax the strain induced by the lattice mismatch between $Ga_{1-x-y}Fe_xNi_ySb$ and GaAs. Compared with AlSb, $Al_{0.9}Ga_{0.1}Sb$ buffer achieves a smoother surface, while the buffer layer keeps insulating due to the low concentration of Ga. After that, a $Ga_{1-x-y}Fe_xNi_ySb$ layer of 100 nm with almost the same Fe concentration x and different Ni concentration y was grown at the growth rate of 0.4 μm/h at 250 °C. Finally, a 2-nm-thick GaSb cap layer was grown at 250 °C to prevent oxidation of underlying $Ga_{1-x-y}Fe_xNi_ySb$ layer. We grew two series of $Ga_{1-x-y}Fe_xNi_ySb$ samples, A1−A4 and B1−B4, and the sample information is listed in Table 1. We changed x of samples A1−A4 (x = 25.2%−29.8%) and kept y = 0, to investigate the magnetic anisotropy and hole mobility of (Ga,Fe)Sb. Samples B1−B4 with nearly constant x (x ≈ 24%) and changed y (y =

Correspondence to: H L Wang, allen@semi.ac.cn
Received 6 AUGUST 2023; Revised 4 SEPTEMBER 2023.

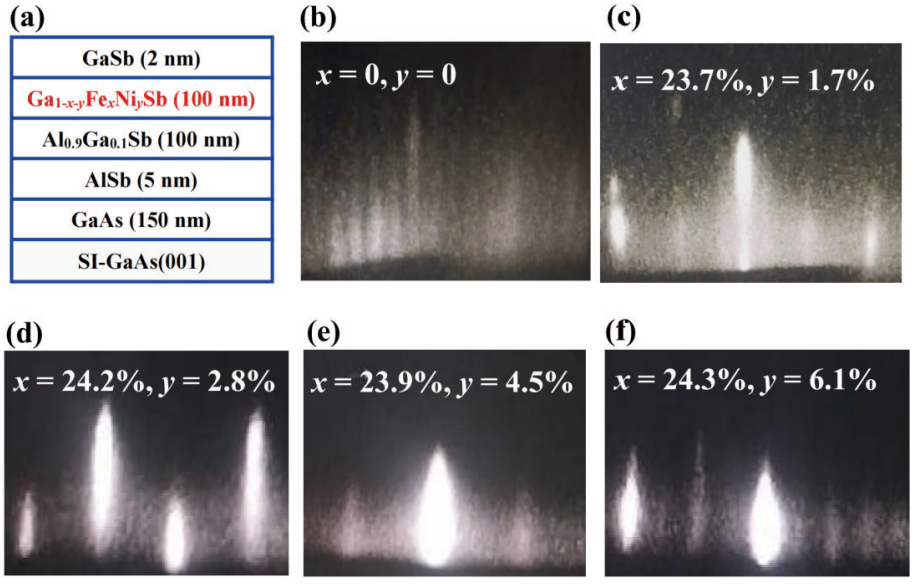

Fig. 1. (Color online) (a) Schematic layer structure of $Ga_{1-x-y}Fe_xNi_ySb$ samples. (b) The RHEED pattern of an undoped GaSb sample. (c)–(f) RHEED patterns taken along the [110] azimuth after the growth of $Ga_{1-x-y}Fe_xNi_ySb$ layers for samples B1–B4 ($x \approx 24\%$, $y = 1.7\%$–6.1%).

Table 1. Curie temperature T_C, hole mobility μ at 10 K, saturation magnetization M_S and anisotropy constant K_u of $Ga_{1-x-y}Fe_xNi_ySb$ films with different Fe concentration x and Ni concentration y.

Sample	x (%)	y (%)	T_C (K)	μ (cm²/(V·s))	M_S (emu/cc)	K_u (erg/cc)
A1	25.2	0	337	6.2	142	-1.8×10^3
A2	26.9	0	351	3.4	144	1.2×10^3
A3	28.0	0	362	1.9	147	4.5×10^3
A4	29.8	0	375	1.1	151	7.6×10^3
B1	23.7	1.7	319	31.3	148	-2.1×10^3
B2	24.2	2.8	336	17.9	152	1.4×10^5
B3	23.9	4.5	343	7.5	159	2.3×10^5
B4	24.3	6.1	354	4.6	165	3.8×10^5

1.7%–6.1%) were used to study the y dependence of the magnetic and electronic properties of $Ga_{1-x-y}Fe_xNi_ySb$ samples. In order to manifest the evolution of K_u and μ of $Ga_{1-x-y}Fe_xNi_ySb$, the x of samples A1–A4 was roughly equal to the sum of x (B1–B4) and y (B1–B4), respectively.

The reflection high-energy electron diffraction (RHEED) was used to observe the surface morphology and crystallinity of the samples. The lattice constant of $Ga_{1-x-y}Fe_xNi_ySb$ layers was investigated by X-ray diffraction (XRD). Scanning transmission electron microscopy (STEM) and selective area electron diffraction (SAED) were employed to characterize the crystal structure and impurity concentration of the $Ga_{1-x-y}Fe_xNi_ySb$ layers. The magnetic and electronic properties of $Ga_{1-x-y}Fe_xNi_ySb$ were separately characterized by superconducting quantum interference device (SQUID) magnetometer and physical property measurement system (PPMS).

3. Results and discussion

3.1. Crystalline properties

The RHEED pattern of an undoped GaSb film grown with the same condition as the $Ga_{1-x-y}Fe_xNi_ySb$ samples is displayed in Fig. 1(b). Figs. 1(c)–1(f) present the RHEED patterns of samples B1–B4 taken along the [1$\bar{1}$0] axis after the growth of $Ga_{1-x-y}Fe_xNi_ySb$ layers. It is obvious that the RHEED patterns of $Ga_{1-x-y}Fe_xNi_ySb$ layers are streaky with surface reconstruction of 1 × 3, which is similar with that of GaSb. The results imply that $Ga_{1-x-y}Fe_xNi_ySb$ layers grown by LT-MBE keep the zinc-blende crystal structure.

XRD spectra of samples A1–A4 are shown in Fig. 2(a), while that of samples B1–B4 are shown in Fig. 2(b), which are both performed using the Cu-K_α radiation (wave length λ = 0.15406 nm). No phases other than $Al_{0.9}Ga_{0.1}Sb$ and $Ga_{1-x-y}Fe_xNi_ySb$ can be observed in the XRD spectra, and in particular there are no Fe–Sb, Ni–Sb intermetallic compounds or metal clusters. The concentration of Fe and Ni is preliminary determined by a series of energy dispersive spectra, which are measured repeatedly at different positions in $Ga_{1-x-y}Fe_xNi_ySb$ layer. According to the dependence between the Fe (Ni) doping concentration and Fe/Ga (Ni/Fe) flux ratio, the x and y could be further confirmed, as listed in Table 1. The lattice constant of (Ga,Fe)Sb and $Ga_{1-x-y}Fe_xNi_ySb$ could be given by $a_1 = (1-x)a_{GaSb} + xa_{FeSb}$ and $a_2 = (0.76-y)a_{GaSb} + 0.24a_{FeSb} + ya_{NiSb}$. Here, a_{GaSb}, a_{FeSb} and a_{NiSb} are the lattice constant of GaSb, hypothetical zinc-blende FeSb and NiSb, respectively, which are estimated to be 0.60648 nm (a_{GaSb}), 0.55027 nm (a_{FeSb}) and 0.58233 nm (a_{NiSb}) as plotted in Figs. 2(c) and 2(d). The results are consistent with previous research[16].

The crystal structure and impurity concentration of samples A1–A4 and B1–B4 were characterized by STEM and SAED. Fig. 3(a) shows the STEM lattice image of sample B4

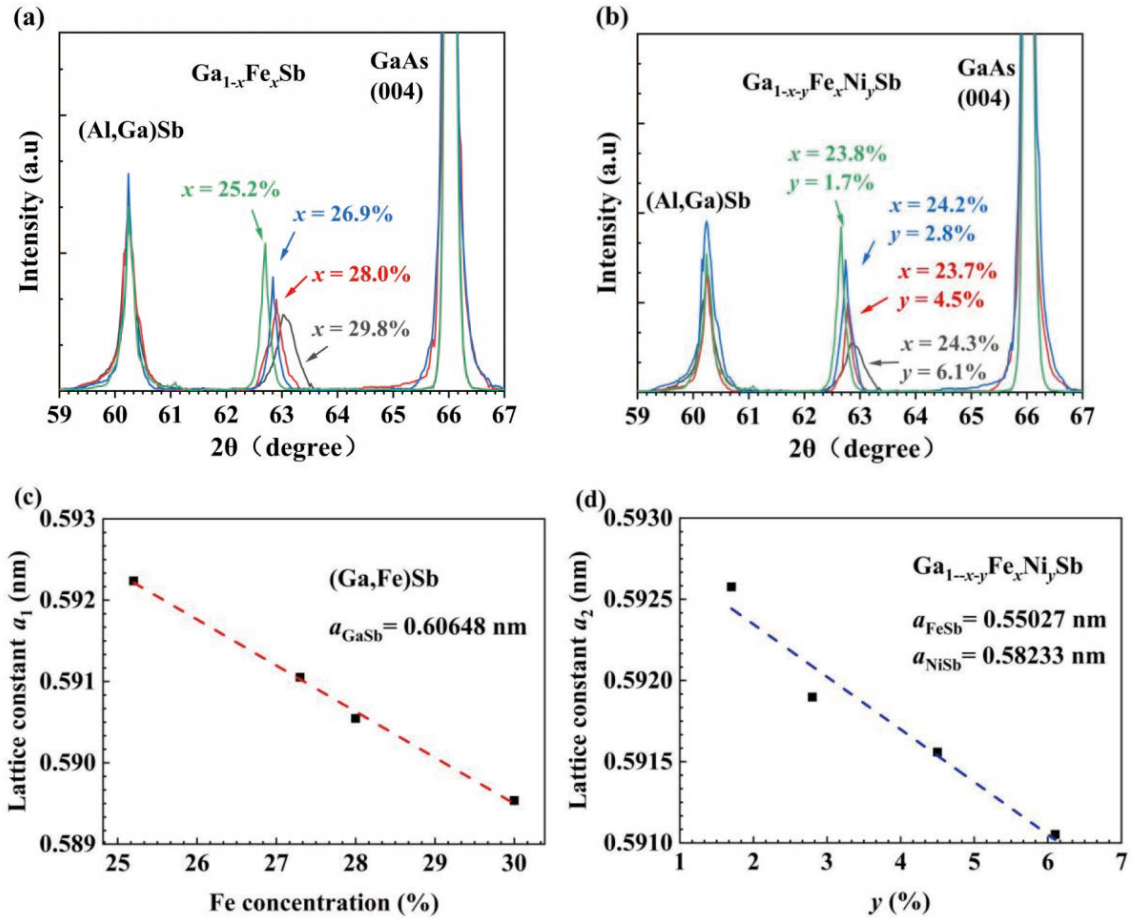

Fig. 2. (Color online) (a) XRD spectra of $Ga_{1-x-y}Fe_xNi_ySb$ samples A1–A4 (x = 25.2%–29.8%, y = 0). (b) XRD spectra of samples B1–B4 ($x \approx 24\%$, y = 1.7%–6.1%). (c) x dependence of the lattice constant of A1–A4. (d) y dependence of the lattice constant of B1–B4.

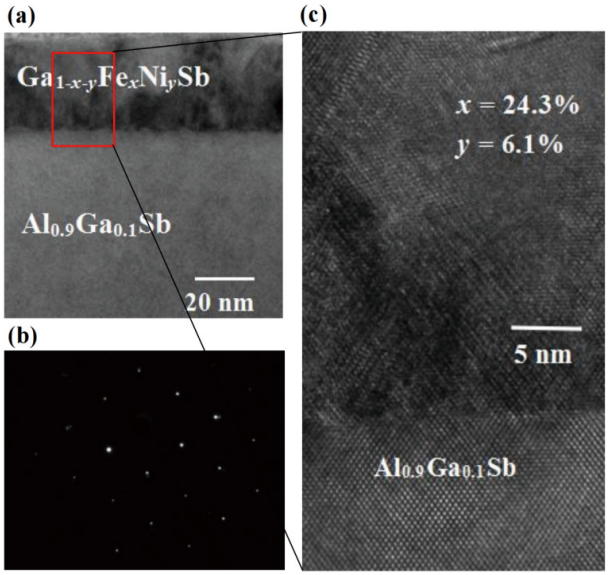

Fig. 3. (Color online) (a) The cross-sectional STEM image of typical $Ga_{1-x-y}Fe_xNi_ySb$ sample B4 (x = 24.3%, y = 6.1%). (b) SAED pattern of the $Ga_{1-x-y}Fe_xNi_ySb$ layers in sample B4. (c) The area marked by red rectangles shown in Fig. 3(a).

taken along the [110] axis, showing the clear interface between $Ga_{1-x-y}Fe_xNi_ySb$ layer and buffer layer. Through the enlarged picture area marked by red rectangle in Fig. 3(a), the crystal structure of $Ga_{1-x-y}Fe_xNi_ySb$ layer is displayed more clearly in Fig. 3(c). Fig. 3(b) shows the SAED pattern of $Ga_{1-x-y}Fe_xNi_ySb$ layer of representative sample B4 (x = 24.3%, y = 6.1%). Due to the nonuniform Fe distribution in sample B4 with high doping concentration[17], the shaded areas in Fig. 3(c) probably are caused by the influence of the strong ferromagnetism. Generally, there are no visible defects in $Ga_{1-x-y}Fe_xNi_ySb$ layer and no phases other than $Ga_{1-x-y}Fe_xNi_ySb$.

3.2. Magnetic properties

A SQUID magnetometer was used to investigate the magnetic properties of $Ga_{1-x-y}Fe_xNi_ySb$ samples. Fig. 4 shows the magnetization hysteresis curves (M–H) of samples B1–B4 ($x \approx$ 24%, y = 1.7%–6.1%) measured at 10 K, with the magnetic field H being applied along the [110] and [001] axes. Clear hysteresis curves are observed and shown in Fig. 4, which demonstrate the presence of ferromagnetic order of $Ga_{1-x-y}Fe_xNi_ySb$ layers. For the samples with y = 1.7%, the in-plane magnetization and perpendicular magnetization show similar characteristics, suggesting small magnetic anisotropy in this sample. For the samples with y = 2.8%–6.1%, the difference between in-plane and perpendicular magnetization is remarkable. The perpendicular magnetization saturates at a much smaller magnetic field than the in-plane magnetization, indicating that the easy axis of magnetization is perpendicular to the plane and there is a strong magnetic anisotropy in these samples. As shown in Fig. 4, the perpendicular saturation magnetic fields of samples B1–B4 are marked by the blue arrows. In addition, the saturation magnetization M_S values increase as y increases, which are 148, 152, 159 and 165 emu/cm^3 at y = 1.7, 2.8, 4.5 and 6.1%. The magnetic anisotropy constant

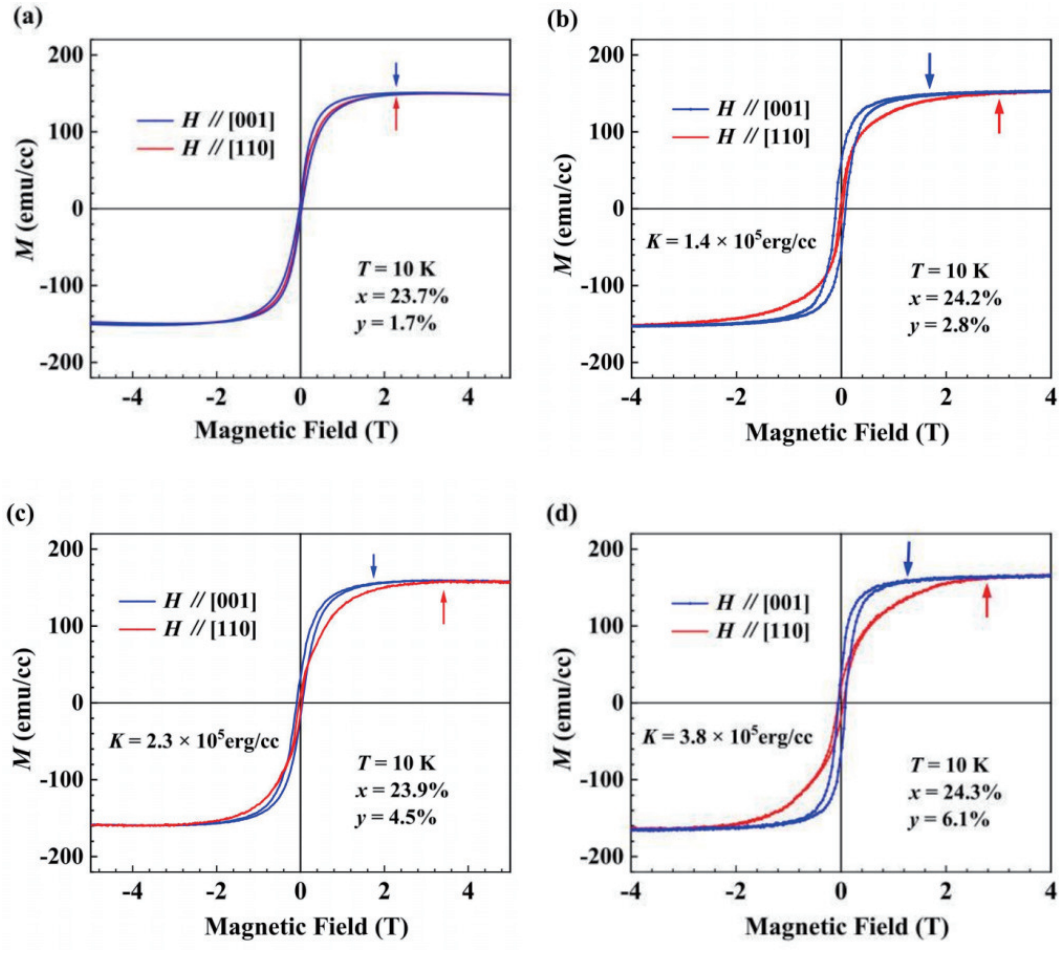

Fig. 4. (Color online) Magnetic hysteresis curves (M–H) measured at 10 K of samples B1–B4 ($x \approx 24\%$, $y = 1.7\%$–6.1%) with a magnetic field applied along the [001] axis and the [110] axis. The blue and red arrows in (a)–(d) signify the perpendicular saturation magnetic fields and the positions of H_S.

could be estimated by $K_u = \int_0^{H_S} (M_\perp - M_{||})\,dH + 2\pi M_S^2$, where $M_\perp$ and $M_{||}$ represent the perpendicular and in-plane magnetization, respectively. Here, the saturation field H_S means the intersection of the in-plane and perpendicular M–H loop, which is marked by the red arrows in Fig. 4. It is found that the K_u is negligible for $y = 1.7\%$ but increases to 2.3×10^5 erg/cm^3 for $y = 4.5\%$ and 3.8×10^5 erg/cm^3 for $y = 6.1\%$, suggesting the improvement of Ni doping to the magnetic anisotropy of $Ga_{1-x-y}Fe_xNi_ySb$. Additionally, the magnetization hysteresis curves of samples A1–A4 ($x = 25.2\%$–29.8%, $y = 0$) show similar characteristics with that of sample B1, of which the K_u can also be neglected. The results imply that Ni doping can effectively improve the magnetic anisotropy of $Ga_{1-x-y}Fe_xNi_ySb$.

3.3. Transport properties

Hall data of samples B1–B4 was collected to characterize the magnetic transport properties of the $Ga_{1-x-y}Fe_xNi_ySb$ films. Samples B1–B4 were fabricated into Hall bars with a size of 200×40 μm^2. The hole mobility of $Ga_{1-x-y}Fe_xNi_ySb$ is determined by $\mu = \dfrac{l\Delta R_{xy}}{w\Delta B R_{xx}}$, where the R_{xy}, R_{xx} , l and w are the anomalous Hall resistance, the longitudinal Hall resistance measured at zero-field, and the length and width between the electrodes of Hall bar, respectively. In order to accurately determine the hole mobility of $Ga_{1-x-y}Fe_xNi_ySb$, the influence of AHE should be excluded. Thus, we measured R_{xy} at low temperature (10 K) and calculated the $\Delta R_{xy}/\Delta B$ at high magnetic field (up to 16 T). As shown in Fig. 5, we measured the magnetic field dependence of Hall resistance curves (R_{Hall}–H) of samples B1–B4 ($x \approx 24\%$, $y = 1.7\%$–6.1%) at 10 K. As plotted in the insets of Fig. 5, the obvious hystereses at low temperature reveal that R_{Hall} is dominated by the AHE in the low magnetic field range. Moreover, the red dashed lines in Fig. 5 almost coincide with the R_{Hall}–H curves at high magnetic fields, implying that the magnetization is nearly saturated. The mobility of $Ga_{1-x-y}Fe_xNi_ySb$ samples B1–B4 ($x \approx 24\%$) is listed in Table 1, which decrease from 31.3 cm^2/(V·s) at $y = 1.7\%$ to 4.6 cm^2/(V·s) at $y = 6.1\%$. As for samples A1–A4 ($y = 0$), μ values also decline from 6.2 cm^2/(V·s) at $x = 25.2\%$ to 1.1 cm^2/(V·s) at $x = 29.8\%$. Both Ni doping and Fe doping would reduce the hole mobility of $Ga_{1-x-y}Fe_xNi_ySb$, however, samples co-doped with Fe and Ni exhibit higher mobility than that doped with Fe solely.

The Curie temperatures of samples B1–B4 ($x \approx 24\%$) are estimated by the Arrott plots of the R_{Hall}–H curves, which rise from 319 K ($y = 1.7\%$) up to 354 K ($y = 6.1\%$). With regard to samples A1–A4, the T_C values of these samples also increase from 337 K at $x = 25.2\%$ to 375 K at $x = 29.8\%$, demonstrating similar impurity concentration dependence characteristics. The effects of Ni doping on mobility and T_C behave similar but weaker than that of Fe doping.

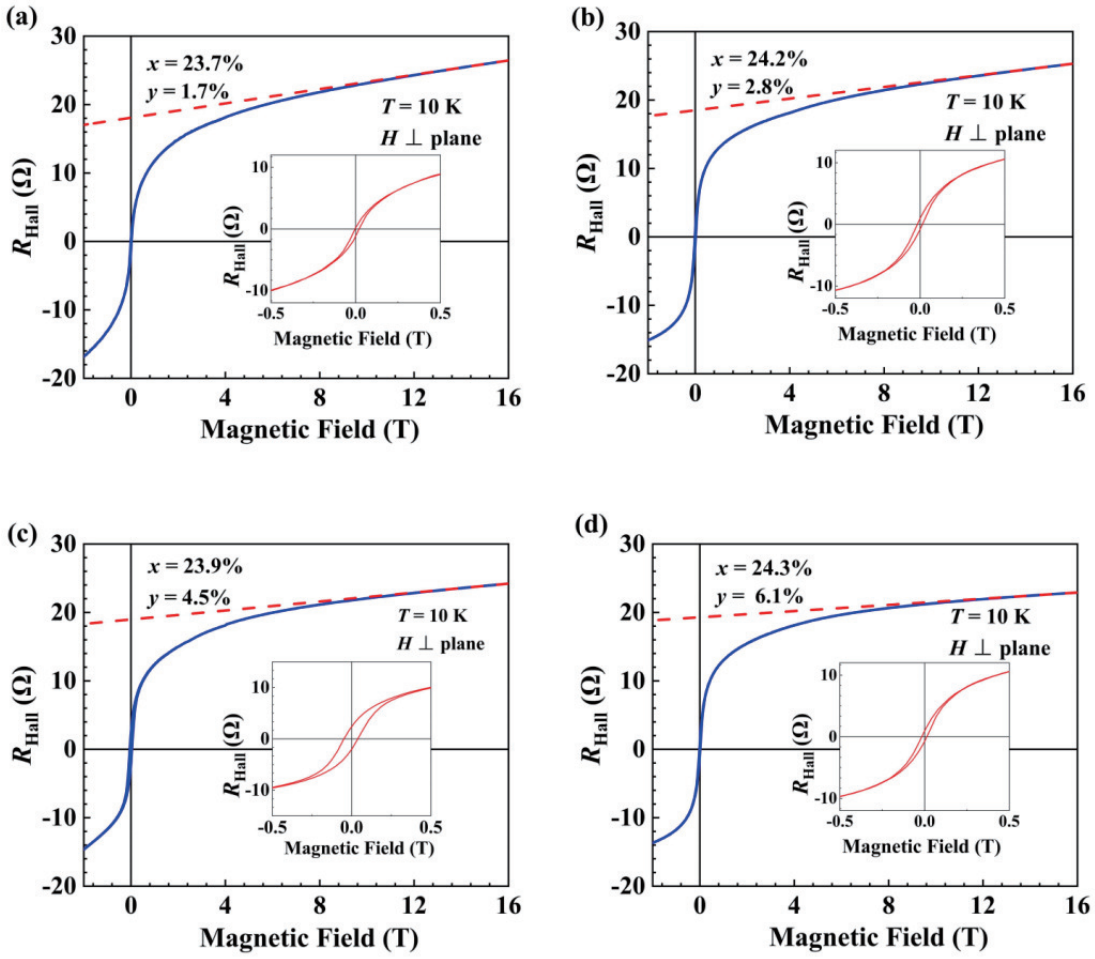

Fig. 5. (Color online) The magnetic field dependence of Hall resistance curves (R_{Hall}–H) of the samples B1–B4 ($x \approx 24\%$, $y = 1.7\%$–6.1%) measured at 10 K.

4. Conclusion

In summary, we co-doped Ni with Fe into GaSb host semiconductor by using LT-MBE, and achieved enhanced magnetic anisotropy and hole mobility of $Ga_{1-x-y}Fe_xNi_ySb$ films compared with that of (Ga,Fe)Sb. XRD and STEM results reveal that there are no second phases in $Ga_{1-x-y}Fe_xNi_ySb$ films. Moreover, we obtained the anisotropy constant K_u (up to 3.8×10^5 erg/cm^3) and hole mobility μ (up to 31.3 cm^2/(V·s)) in $Ga_{1-x-y}Fe_xNi_ySb$ films, which are much higher than that of (Ga,Fe)Sb (with the maximum $K_u = 7.6 \times 10^3$ erg/cm^3 and maximum μ = 6.2 cm^2/(V·s)). Our results indicate that $Ga_{1-x-y}Fe_xNi_ySb$ is a promising magnetic semiconductor for spintronic applications.

Acknowledgments

This work is supported by the National Key R&D Program of China (No. 2021YFA1202200), the CAS Project for Young Scientists in Basic Research (No. YSBR-030), and the National Natural Science Foundation Program of China (No. 12174383). H L Wang also acknowledges the support from the Youth Innovation Promotion Association, Chinese Academy of Sciences (No. 2021110).

Appendix A. Supplementary material

Supplementary materials to this article can be found online at https://doi.org/10.1088/1674-4926/45/1/012101.

References

[1] Ohno H. Making nonmagnetic semiconductors ferromagnetic. Science, 1998, 281, 951
[2] Dietl T, Ohno H, Matsukura F, et al. Zener model description of ferromagnetism in zinc-blende magnetic semiconductors. Science, 2000, 287, 1019
[3] Chiba D, Sawicki M, Nishitani Y, et al. Magnetization vector manipulation by electric fields. Nature, 2008, 455, 515
[4] Jungwirth T, Wunderlich J, Novák V, et al. Spin-dependent phenomena and device concepts explored in (Ga, Mn)As. Rev Mod Phys, 2014, 86, 855
[5] Dietl T, Ohno H. Dilute ferromagnetic semiconductors: Physics and spintronic structures. Rev Mod Phys, 2014, 86, 187
[6] Ohno H, Munekata H, Penney T, et al. Magnetotransport properties of *p*-type (In, Mn)As diluted magnetic III-V semiconductors. Phys Rev Lett, 1992, 68, 2664
[7] Koshihara S, Oiwa A, Hirasawa M, et al. Ferromagnetic order induced by photogenerated carriers in magnetic III-V semiconductor heterostructures of (In, Mn)As/GaSb. Phys Rev Lett, 1997, 78, 4617
[8] Akai H. Ferromagnetism and its stability in the diluted magnetic semiconductor (In, Mn)As. Phys Rev Lett, 1998, 81, 3002
[9] Oiwa A, Endo A, Katsumoto S, et al. Magnetic and transport properties of the ferromagnetic semiconductor heterostructures (In, Mn)As/(Ga, Al)Sb. Phys Rev B, 1999, 59, 5826
[10] Schallenberg T, Munekata H. Preparation of ferromagnetic (In, Mn)As with a high Curie temperature of 90K. Appl Phys Lett, 2006, 89, 042507

[11] Ohno H, Shen A, Matsukura F, et al. (Ga, Mn)As: A new diluted magnetic semiconductor based on GaAs. Appl Phys Lett, 1996, 69, 363
[12] Matsukura F, Ohno H, Shen A, et al. Transport properties and origin of ferromagnetism in (Ga, Mn)As. Phys Rev B, 1998, 57, R2037
[13] Chen L, Yang X, Yang F H, et al. Enhancing the curie temperature of ferromagnetic semiconductor (Ga, Mn)As to 200 K via nanostructure engineering. Nano Lett, 2011, 11, 2584
[14] Wang H L, Ma J L, Zhao J H. Giant modulation of magnetism in (Ga, Mn)As ultrathin films via electric field. J Semicond, 2019, 40, 092501
[15] Wang H L, Ma J L, Wei Q Q, et al. Mn doping effects on the gate-tunable transport properties of Cd_3As_2 films epitaxied on GaAs. J Semicond, 2020, 41, 072903
[16] Tu N T, Hai P N, Anh L D, et al. (Ga, Fe)Sb: A p-type ferromagnetic semiconductor. Appl Phys Lett, 2014, 105, 132402
[17] Tu N T, Hai P N, Anh L D, et al. Magnetic properties and intrinsic ferromagnetism in (Ga, Fe)Sb ferromagnetic semiconductors. Phys Rev B, 2015, 92, 144403
[18] Tu N T, Hai P N, Anh L D, et al. High-temperature ferromagnetism in heavily Fe-doped ferromagnetic semiconductor (Ga, Fe)Sb. Appl Phys Lett, 2016, 108, 192401
[19] Goel S, Anh L D, Ohya S, et al. Ferromagnetic resonance and control of magnetic anisotropy by epitaxial strain in the ferromagnetic semiconductor ($Ga_{0.8}$, $Fe_{0.2}$)Sb at room temperature. Phys Rev B, 2019, 99, 014431
[20] Goel S, Anh L D, Ohya S, et al. In-plane to perpendicular magnetic anisotropy switching in heavily-Fe-doped ferromagnetic semiconductor (Ga, Fe)Sb with high Curie temperature. Phys Rev Materials , 2019, 084417
[21] Tu N T, Hai P N, Anh L D, et al. High-temperature ferromagnetism in new n-type Fe-doped ferromagnetic semiconductor (In, Fe)Sb. Appl Phys Express, 2018, 11, 063005
[22] Nguyen T T, Pham N, Le D, et al. Electrical control of ferromagnetism in the n-type ferromagnetic semiconductor (In, Fe)Sb with high Curie temperature. Appl Phys Lett, 2018, 112, 122409
[23] Nguyen T T, Pham N H, Le D A, et al. Heavily Fe-doped n-type ferromagnetic semiconductor (In, Fe)Sb with high Curie temperature and large magnetic anisotropy. 2019 Compound Semiconductor Week (CSW), Nara, Japan, 2019, 1
[24] Sakamoto S, Tu N T, Takeda Y, et al. Electronic structure of the high-T_C ferromagnetic semiconductor (Ga, Fe)Sb: X-ray magnetic circular dichroism and resonance photoemission spectroscopy studies. Phys Rev B, 2019, 100, 035204
[25] Sriharsha K, Anh L D, Tu N T, et al. Magneto-optical spectra and the presence of an impurity band in *p*-type ferromagnetic semiconductor (Ga, Fe)Sb with high Curie temperature. APL Mater, 2019, 7, 021105
[26] Tanaka M. Recent progress in ferromagnetic semiconductors and spintronics devices. Jpn J Appl Phys, 2021, 60, 010101
[27] Stefanowicz W, Śliwa C, Aleshkevych P, et al. Magnetic anisotropy of epitaxial (Ga, Mn)As on (113)A GaAs. Phys Rev B, 2010, 81, 155203

Zhi Deng obtained his B.E. degree from Center of Materials Science and Optoelectronics Engineering in 2020 at University of Chinese Academy of Sciences. He then joined the State Key Laboratory of Superlattices and Microstructures under the supervision of Prof. Jianhua Zhao. His research focuses on Fe-based $\mathrm{III}-\mathrm{V}$ magnetic semiconductors.

Hailong Wang received his B.Sc. degree from the School of Physics of Peking University in 2009, and a PhD degree from the University of Chinese Academy of Sciences in 2014. From 2014 to 2016, he was a postdoc at the Institute of Physics in Chinese Academy of Sciences, and then worked in the Institute of Semiconductors in Chinese Academy of Sciences. His current interests include $\mathrm{III}-\mathrm{V}$ magnetic semiconductors, semiconductor two-dimensional electron gas and magnetic metal/semiconductor heterostructures.